


Highly CO₂-Selective Organic Molecular Cages: What Determines the CO₂ Selectivity

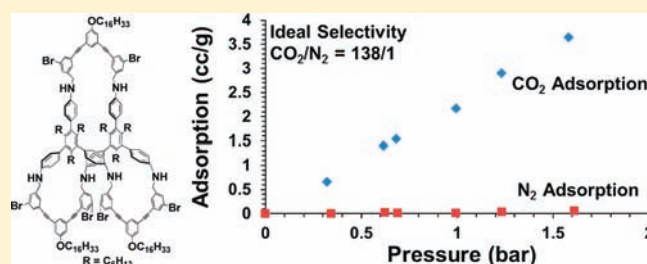
Yinghua Jin,[†] Bret A. Voss,[‡] Athena Jin,[†] Hai Long,[§] Richard D. Noble,[‡] and Wei Zhang^{*,†}

[†]Department of Chemistry and Biochemistry and [‡]Department of Chemical and Biological Engineering, University of Colorado, Boulder, Colorado 80309, United States

[§]National Renewable Energy Laboratory, Golden, Colorado 80401, United States

 Supporting Information

ABSTRACT: A series of novel organic cage compounds 1–4 were successfully synthesized from readily available starting materials in one-pot in decent to excellent yields (46–90%) through a dynamic covalent chemistry approach (imine condensation reaction). Covalently cross-linked cage framework 14 was obtained through the *cage-to-framework* strategy via the Sonogashira coupling of cage 4 with the 1,4-diethynylbenzene linker molecule. Cage compounds 1–4 and framework 14 exhibited exceptional high ideal selectivity (36/1–138/1) in adsorption of CO₂ over N₂ under the standard temperature and pressure (STP, 20 °C, 1 bar). Gas adsorption studies indicate that the high selectivity is provided not only by the amino group density (mol/g), but also by the intrinsic pore size of the cage structure (distance between the top and bottom panels), which can be tuned by judiciously choosing building blocks of different size. The systematic studies on the structure–property relationship of this novel class of organic cages are reported herein for the first time; they provide critical knowledge on the rational design principle of these cage-based porous materials that have shown great potential in gas separation and carbon capture applications.



INTRODUCTION

Three-dimensional (3-D) shape-persistent cage compounds have attracted considerable attention due to their important applications as sensors, nanoreactors, delivery vehicles, gas storage, and separation materials.^{1–5} The syntheses of nanosized cage compounds based on supramolecular chemistry, such as metal–ligand coordination or hydrogen-bonding interactions, are well advanced, and numerous fascinating molecular architectures and their applications utilizing the internal voids have been demonstrated.^{1–8} However, analogous covalently assembled cage molecules, which are thermally and chemically more robust, are relatively uncommon, mainly because of the synthetic challenge of constructing them via irreversible chemical transformations (e.g., multistep, time-consuming synthesis, low overall yield). In this context, dynamic covalent chemistry (DCC)^{9,10} using reversible covalent bond formation has emerged as a powerful tool for construction of sophisticated covalently linked nanostructures. Analogous to supramolecular chemistry, DCC is thermodynamically controlled, thus, presenting self-correction behavior and generating the most thermodynamically stable molecular assembly under appropriate conditions. Reversible metathesis (imine, olefin, or alkyne) and boronic acid condensation reactions have led to successful syntheses of 2-D and 3-D covalently linked discrete organic assemblies as well as frameworks.^{11–16} Herein, we report dynamic covalent

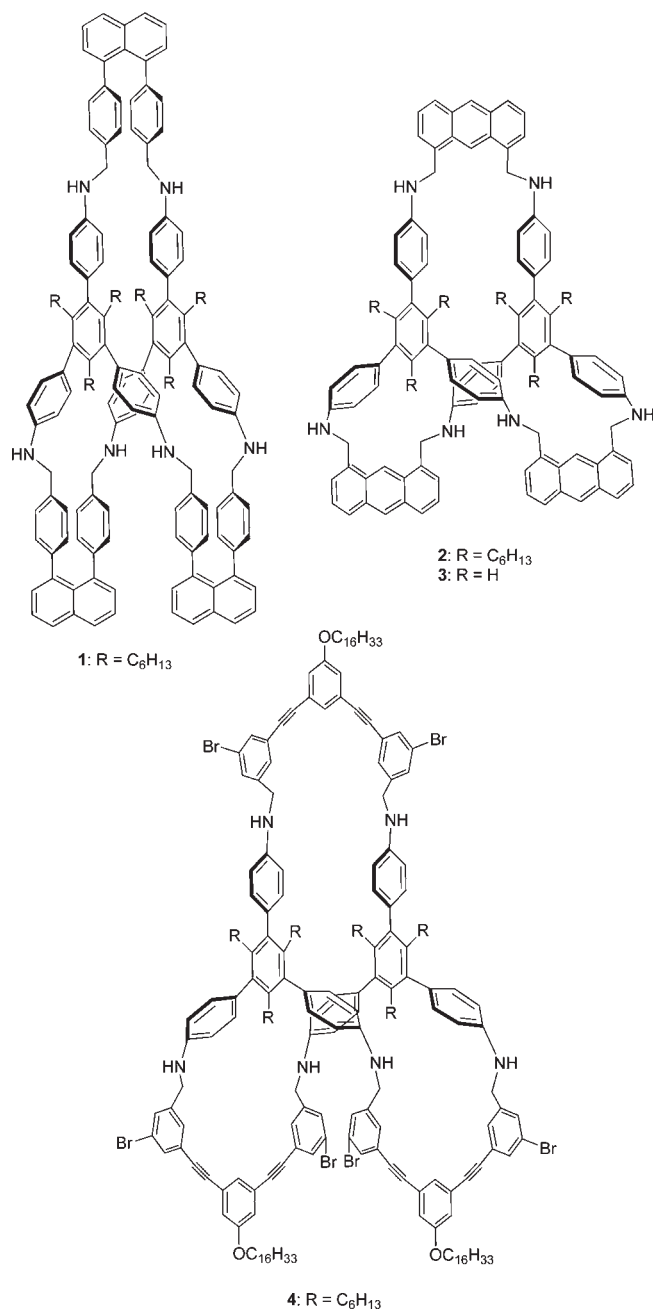
assemblies of a series of novel prismatic cage molecules, which share similar cavity geometry, but exhibit different cavity sizes and presumably also different accessibility for certain gas molecules.

The fundamental motivation for synthesizing these cage molecules with internal voids is to develop a novel class of porous materials suitable for gas adsorption and separation, especially for CO₂/N₂ separation (carbon capture).¹⁷ In the gas adsorption arena, one of the grand challenges is to design and synthesize materials with outstanding gas separation selectivity. Metal-organic-frameworks (MOFs), a class of porous materials consisting of metal ions and organic ligands, have been extensively studied in the past decade.^{18–22} Covalent organic frameworks (COFs)^{23–26} containing only light elements have also been developed in recent years and show great promise as low-density gas storage materials. Conversely, there are only few precedents for discrete molecular organic solids^{27–33} that are known to have gas adsorption behavior. Although some organic solids exhibit good adsorption selectivity for CO₂ over N₂, surprisingly little information is available on the structure–property relationship of these organic compounds. One of our goals is to understand the structure–function relationship, which will

Received: December 2, 2010

Published: April 07, 2011

enable the molecular-level rational design of these types of materials.



In contrast to the generally low solubility of MOFs and COFs, purely organic-based cage molecules are highly soluble in a variety of solvents, thus, allowing easy fabrication of membranes or hybrid composite materials for gas separation applications. It should also be noted that the property of the bulk porous materials assembled from such cage molecules can be easily tuned by varying the size and/or functionality of the cage components. Such a bottom-up *cage-to-framework* strategy would allow for a variety of organic-cage-based porous materials with well-controlled pore size and surface functionality to be realized. Previously, we demonstrated a 3-D shape-persistent trigonal prismatic molecular cage (2) can be efficiently constructed via imine condensation/metathesis in one pot from readily accessible

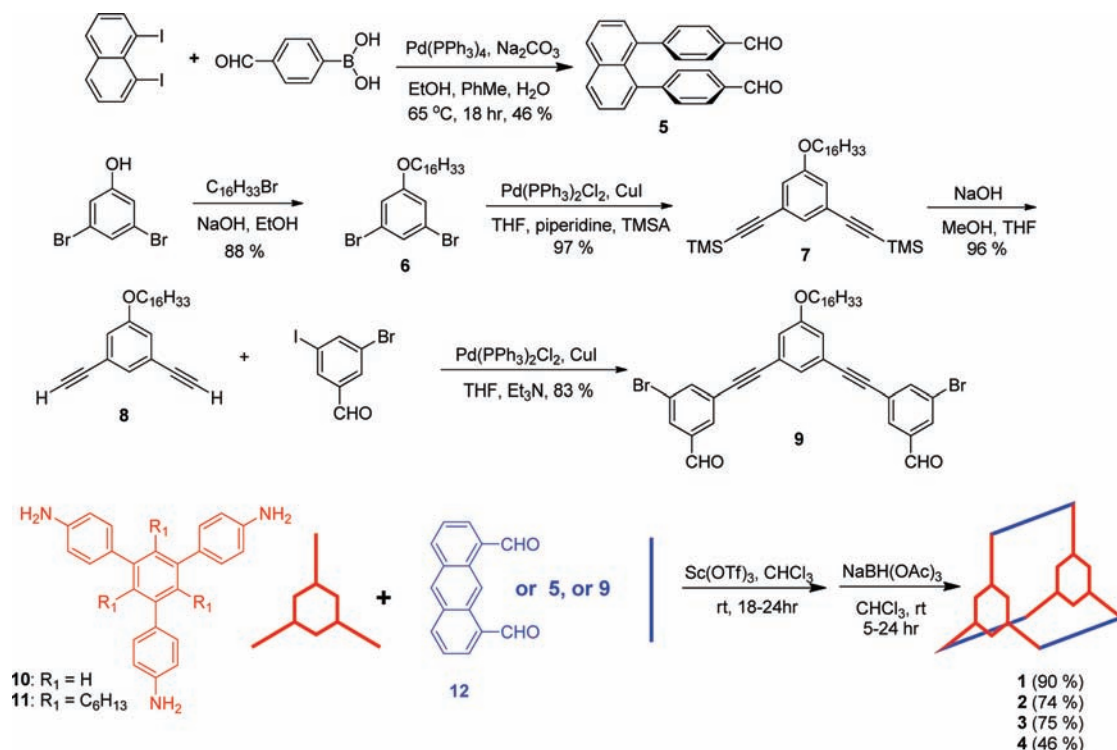
building blocks, and this molecular-cage-based porous crystalline material exhibited an excellent adsorption selectivity (>73/1) for CO₂ over N₂ under ambient conditions (20 °C, 1 bar).³² Gas adsorption was observed to be fully reversible at 20 °C via pressure swings. Although our previous studies showed very encouraging results on utilizing the well-defined, rigid molecular cage in CO₂/N₂ separation, some fundamental questions still remained to be answered, such as what design parameters are critical for these molecular cages to achieve efficient gas separation? Is the gas adsorption selectivity dependent on the intrinsic pore size of the cages? Will cross-linking of these cage building blocks lead to porous framework materials with higher capacity? To explore the high efficiency and versatility of DCC in constructing structure-tunable 3-D organic molecular cages, and also to investigate the key parameters affecting the gas adsorption behavior of these cage molecules, we systematically studied the structure–property relationship of a series of trigonal prismatic cages in gas adsorption capabilities. Our study showed the general applicability of DCC in constructing molecular trigonal prisms and the great tunability of the resulting porous materials toward gas adsorption. Excellent ideal selectivities (up to 138/1) in adsorption of CO₂ over N₂ were observed for these molecular-cage-based porous materials.

RESULTS

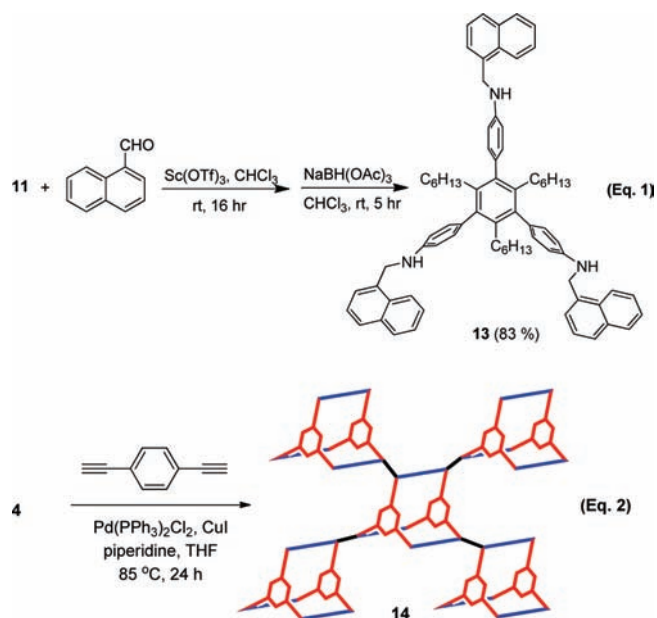
Syntheses of Molecular Cages and a Cage Framework.

Our previous study showed that the intrinsic porosity of the molecular cage structure is critical to achieving high ideal selectivity in gas adsorption.³² To gain some insight into the dependence of gas adsorption on the pore size of a molecular cage, we synthesized a series of trigonal prisms with internal cavities of different size (Scheme 1). The cage compounds 1–4 were synthesized through a one-pot reversible imine condensation/metathesis reaction between triamines (10 or 11) and dialdehydes (5, 9, or 12), followed by hydride reduction of imine bonds to amines. Triamine moieties serve as top and bottom panels of the trigonal prism and dialdehyde moieties serve as the three lateral edges. Presumably, cage 1 consisting of 1,8-bis(4-formylphenyl)naphthalene (5) side pieces contains the smallest pore, while cage 4 containing *m*-phenyleneethynylene moieties has a much larger intrinsic pore volume. Cage 3 without any side chains was designed to study the effect of side chains on the gas adsorption behavior (through comparison with cage 2). 1,8-Bis(4-formylphenyl)naphthalene (5) was prepared from 1,8-diiodonaphthalene through Suzuki coupling. The dialdehyde 9 was synthesized from 3,5-dibromophenol via alkylation, Sonogashira coupling, and desilylation, followed by the final Sonogashira coupling between the diethynyl-substituted intermediate 8 and 3-bromo-5-iodobenzaldehyde. Imine condensation reactions between triamines and dialdehydes were conducted in chloroform under the catalysis of Sc(OTf)₃ at room temperature to form imine-linked cage assemblies. ¹H NMR spectra and gel permeation chromatography (GPC, Figure 1) analyses of the crude products indicated the high conversion (>90%) of the starting materials to the desired cage compounds with a trace amount of high molecular weight oligomers. One-pot reduction of imine-linked cages that were generated in situ yielded compounds 1–4 in moderate to excellent yields (46–90%). The cage molecules (1, 2, and 4) show excellent solubility in a variety of commonly used organic solvents (e.g., CHCl₃, CH₂Cl₂, THF, ethyl acetate). Cage 3 without any alkyl chains has slightly lower solubility in the above-mentioned solvents.

Scheme 1. Syntheses of Molecular Cages 1–4 via Imine Condensation Reaction



Additionally, in order to further investigate the effect of the intrinsic porosity of the molecular cage structure on gas adsorption properties, we synthesized a noncage substrate **13** through reacting top panel **11** with 3 equiv of 1-naphthaldehyde under the imine condensation condition followed by the one-pot hydride reduction (eq 1).



Sonogashira coupling between cage **4** and 1,4-diethynylbenzene (eq 2) led to a red-brown gel-like substance that was washed with organic solvents, vacuum-dried, and crushed

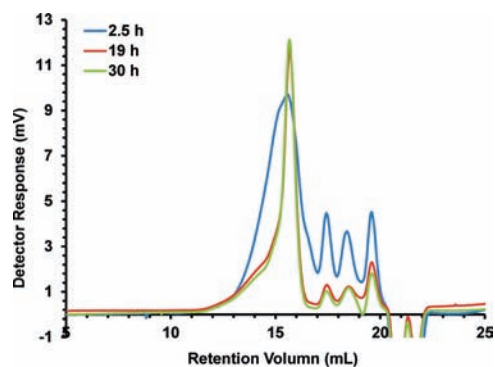


Figure 1. Progress of covalent assembly of cage **4** through imine metathesis as monitored by GPC (THF, 20 °C): Imine condensation/metathesis reaction between the two building units (**9** and **11**) initially generated a series of intermediate oligomeric species as expected (blue curve, 2.5 h). However, the intermediate species were in equilibrium to one another and only the prismatic cage became predominant after 19 h (red and green curves).

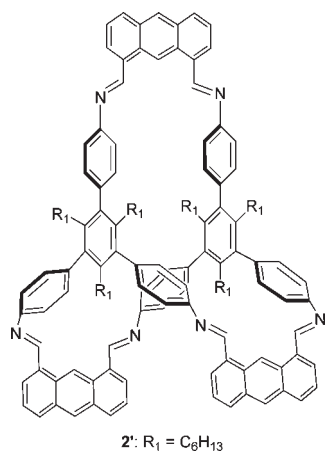
into powder. The ^{13}C cross-polarization magic angle spinning (CP-MAS) NMR spectrum of framework **14** shows resonances at 156 and 89 ppm (Supporting Information), which can be assigned to the bromo-substituted aromatic carbons and the acetylene carbons, respectively. The integration ratio of 1:6 of these two types of carbon atoms indicates about 50% conversion of the bromo functional groups initially present in cage **4**. Covalently connected, cage-based framework structure **14**, insoluble in common organic solvents (e.g., THF, CHCl_3 , CH_2Cl_2 , EtOAc), was compared to non-cross-linked discrete cage molecule **4** in terms of thermal stability, gas adsorption selectivity, and gas uptake capacity.

Characterization of the Molecular Cages and Framework.

As-synthesized molecular cages were obtained by removal of the solvents under vacuum. Discrete cage molecules **1–4** and cage framework **14** were characterized by X-ray powder diffraction (XRD, Figure S3). Cage **2** and framework **14** exhibit some crystalline features, while the others are amorphous with only minor crystallinity.

Characterized by thermogravimetric analysis (TGA), cage compounds (**1–3**) showed exceptionally high thermal stability ($T_{\text{dec}} > 690$ K) compared to many other organic molecular porous materials and MOFs.^{28–35} Cage **4** shows the lowest thermal stability, with a decomposition temperature around 640 K. The cross-linked cage framework **14** showed a weight loss (24%) between 474 K and its decomposition temperature 694 K.³⁶

The morphologies of the porous materials based on cages **1–4**, **14**, and imine-linked cage **2'** were characterized with scanning electron microscope (SEM, Figure 2). Samples of cages **1** and **4** exhibit a sheet-like morphology with little evidence of mesopores or macropores on the surfaces, while cage **2** shows a large number of isolated pores on its surface. Samples of cages **3** and **2'** are composed of porous agglomerates consisting of several micrometer-sized particles, and the morphology of cross-linked cage framework **14** is almost featureless.



Gas Adsorption Study. The ideal selectivity in CO_2/N_2 adsorption was measured at 20 °C by using a specifically designed instrument (Figure S1) for low-pressure gas adsorption with a small amount of samples. Cage samples for the gas adsorption study were prepared by direct removal of the solvent under high vacuum to give mostly amorphous materials. Only cage **2** and cage framework **14** showed some degree of crystallinity. All the cage molecules and the cage framework showed excellent selectivities (36/1–138/1, Figure 3, Table 1) in adsorption of CO_2 over N_2 , with cage **4** showing the highest selectivity (138/1) which is significantly higher than what we previously observed for anthracene-based molecular cage **2**.^{32,37} To our knowledge, these ideal selectivities are the highest reported to date under STP conditions for discrete organic molecules. Cage framework **14** showed an adsorption selectivity of 63/1, which is lower than the corresponding noncross-linked cage **4**. The adsorption capacity of CO_2 (mol %) was found to be similar for all the cages (**1–4**) with small variations (0.31–0.37 mol/mol). The calculated CO_2 weight percentages of these cages are 0.42–1.02%, which is comparable to other previously reported organic solids (e.g., 0.5 wt % for 1,2-dimethoxy-*p*-*tert*-butylcalix-[4]dihydroxyquinone at 298 K, 640 Torr,³⁸ or 0.5 mol/mol for

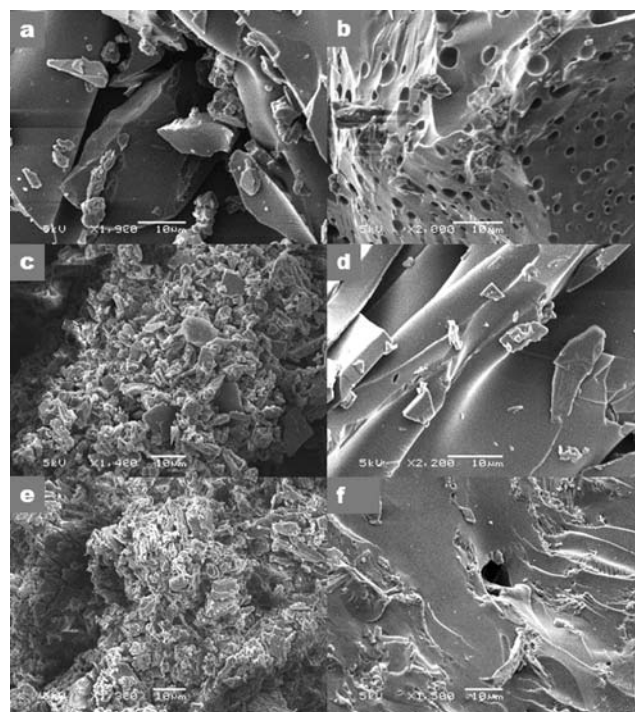


Figure 2. Scanning electron microscope (SEM) images (scale bar = 10 μm): (a) cage **1**; (b) cage **2**; (c) cage **3**; (d) cage **4**; (e) cage **2'**; (f) cage framework **14**.

tris-*o*-phenylenedioxy-cyclotriphosphazene at 298 K, 640 Torr³⁰). A few organic cages have been reported to have higher adsorption capacities of CO_2 (e.g., 11 wt % for noria,^{28c} at 298 K, 1 bar; 9.4 wt % for salicylbisimine cage at 273 K,³³ 1 bar, and 13.2 wt % for imine-linked tetrahedral cage at 275 K, 1.12 bar,²⁹) albeit still relatively low compared to MOFs and COFs.^{39,40} The CO_2 uptake of **13** is 0.18 mol/mol, which is about 2 times less than that of other cage compounds (**1–4**). However, it should be noted that **13** is a noncage analogue and only has three secondary amine groups (vs six amino groups for each closed cage) in the molecule. Cross-linked cage framework **14** shows 4 times higher CO_2 adsorption capacity than that of other cage materials presented here. In all cases, under the STP condition, the N_2 uptake is extremely low, and varies substantially (0.0024–0.0094 mol/mol) depending on the cage dimensions. Similar to the case of CO_2 adsorption, the cage framework **14** showed the largest N_2 uptake (0.0194 mol/mol).

DISCUSSION

Cage Synthesis and Solubility Concern. To obtain a molecular cage with a small intrinsic pore, initially we chose 1,8-diformylnaphthalene as the three side arms of the molecular trigonal prism. Unfortunately, we failed to obtain the pure product in the following multiple trials: Oxidation (pyridinium chlorochromate, or Swern oxidation) of 1,8-bis(hydroxymethyl)naphthalene provided an oxidative lactonization product or a trace amount of monoaldehyde; reduction of 1,8-dicyanonaphthalene using DIBAL-H or Raney-Ni yielded only unknown species; ozonolysis of acenaphthylene afforded 1,3-dimethoxy-1*H*,3*H*-naphtho[1,8-*cd*]pyran predominantly, and the reaction of this dimethoxy acetal derivative with triamine **11** under the imine condensation conditions ($\text{Sc}(\text{OTf})_3$, CHCl_3 , 75 °C, 48 h) failed to give the cage product. Given the problematic synthesis of

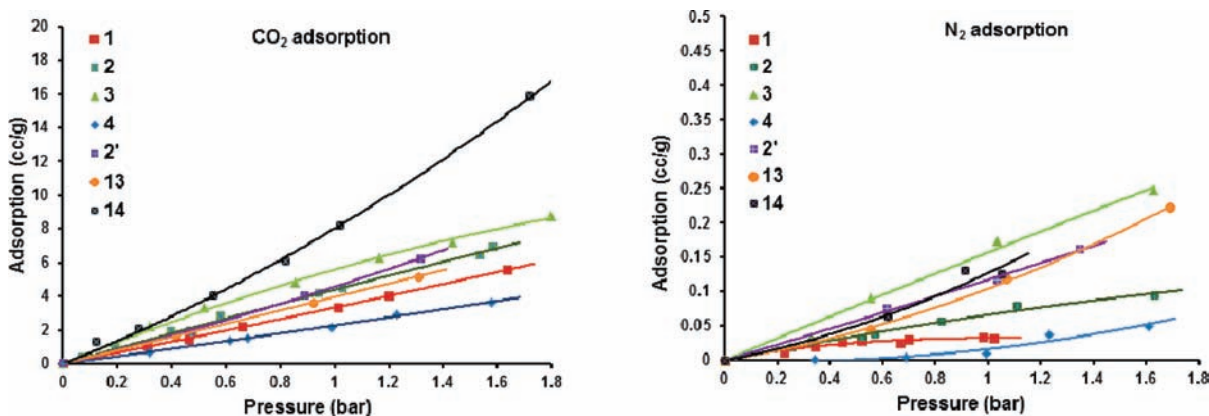
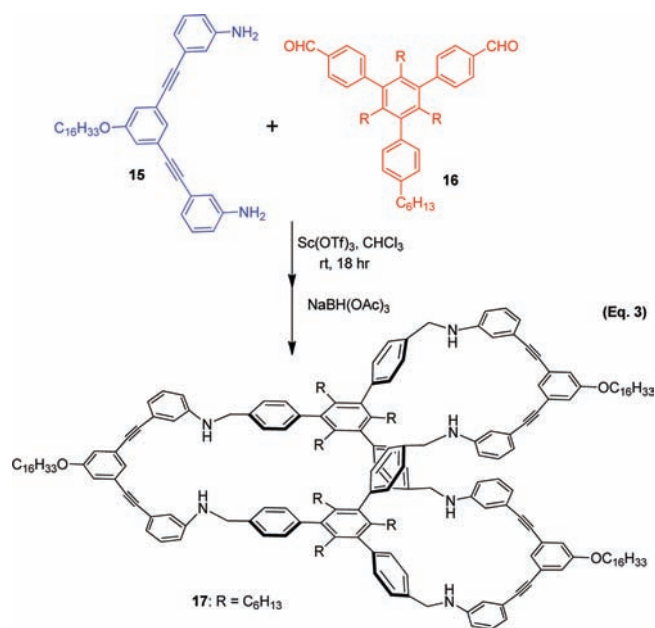


Figure 3. The adsorption isotherms of CO₂ and N₂ for cages 1–4, 2', compound 13, and cage framework 14.

1,8-diformylnaphthalene, later we designed compound 5 as an alternative side building block, and imine condensation between 5 and 11 led to the successful formation of prismatic cage 1.

The syntheses of the prismatic cages are greatly facilitated by utilizing one-step, high-yielding dynamic covalent chemistry. The reversible nature of imine metathesis overcomes kinetically introduced, undesired bond formation, and provides the most thermodynamically favored product at equilibrium. Covalent assemblies of the prismatic cages presented here were monitored by ¹H NMR and/or gel permeation chromatography (GPC, Figure 1). For example, imine condensation reaction between the trigonal panel 11 and lateral edge 9 initially generated a series of intermediate oligomeric species as expected, which was confirmed by the observation of a rather broad peak in GPC trace of the crude reaction mixtures after 2.5 h (Figure 1, blue line). However, all the possible intermediates were in equilibrium to one another and only the trigonal prismatic cage compound, which is enthalpy-favored because of no angle strain and also entropy-favored due to consisting of minimum number of building units, became predominant at equilibrium (after 19 h).



Since the prismatic cage structures are constructed with high efficiency in a modular fashion through DCC, this method allows

systematic tuning of their pore size and functionality with great ease. Simply varying the size and geometry of the top-bottom building blocks and/or side pieces (e.g., 5, 9, or 12) leads to the formation of a series of nanoporous materials with different pore volumes. The flexible functional group choice (amine vs aldehyde) of imine bonding partners further facilitates the synthetic accessibility of building blocks. For example, top and bottom panels of the cage could be substituted with aldehydes (16) instead of amines and the three lateral edges could contain complementary amino groups (15). Imine condensation between 15 and 16 worked as well as the reaction between 11 and 9, and molecular cage 17 was obtained in a good yield (45%, eq 3), comparable to the synthesis of 4. This model study shows the versatility of the imine condensation approach in molecular cage synthesis, thus, offering more options for the design and syntheses of cage building blocks.

In contrast to the good solubility (>20 mg/mL) of molecular cage 1, 2, and 4 in various solvents (e.g., THF, EtOAc, CHCl₃, CH₂Cl₂), the unsubstituted cage 3 shows a relatively poor solubility (5 mg/mL in CHCl₃), especially the imine-linked intermediate before hydride reduction (<1 mg/mL in CHCl₃). During the imine condensation reaction, a large amount of precipitates formed within 2 h. ¹H NMR characterization of the solution phase only showed a trace amount of cage product, indicating the poor solubility of imine intermediates. After subjecting the precipitates to further hydride reduction, the target cage compound 3 was obtained in a high yield (75%). Presumably, the formation of the imine-linked cage intermediate is predominant in the first stage (imine condensation), which may be due to the following two possibilities: (1) high selectivity in direct cage formation over polymer/oligomer formation; (2) lower solubility of the imine cage than other polymer/oligomer intermediates, thus, precipitation shifting the equilibrium. However, the rationale for the above two possibilities are still open to speculation.

Cage Framework Structure. The ability to produce ordered, 3-D framework materials with precise control of their chemical and molecular structures would allow manipulation of the material composition through the “bottom-up” approach to develop novel materials with unprecedented physical properties (e.g., mechanical, thermal, electrical, magnetic, etc.). The pore size and surface functional group are the two key parameters determining the chemical and physical properties of the resulting 3-D framework materials. Conventionally, well-defined 3-D frameworks have been achieved through metal-coordination or

Table 1. Gas adsorption capacity and selectivity of cages 1-4, 2', compound 13, and cage framework 14

compound	CO ₂ adsorption (1 bar, 20 °C)			N ₂ adsorption (1 bar, 20 °C)		pore size (Å) ^a	ideal selectivity CO ₂ /N ₂
	Wt %	cc/g	mol/mol	cc/g	mol/mol		
1	0.61	3.32	0.31	0.033	0.0031	6.03	100
2	0.80	4.35	0.36	0.065	0.0053	6.27	67
3	1.02	5.58	0.33	0.157	0.0092	6.72	36
4	0.45	2.27	0.33	0.016	0.0024	5.27	138
2'	0.84	4.56	0.37	0.117	0.0094	7.32	39
13	0.72	3.95	0.18	0.104	0.0048	-	38
14	1.57	8.01	1.22	0.127	0.0194	-	63

^a Pore sizes (distance between the top and bottom panels) were obtained from the energy-minimized molecular modeling.

hydrogen-bonding driven self-assembly of 1-D or 2-D building units. As a novel alternative approach, we show that well-defined, ordered purely organic frameworks can be constructed by covalently linking 3-D cage building blocks containing predefined molecular pores. Such a “cage-to-framework” strategy would enable efficient encoding of both dimensional (pore size/distribution) and functional information (guest recognition, sensing, catalysis, etc.) within the individual cage molecule into the final frameworks.⁴¹ The coupling reaction between cage 4 and divalent linker molecule 1,4-diethynylbenzene thus served as a model study to test the feasibility of such a “cage-to-framework” strategy. The ¹³C cross-polarization magic angle spinning (CP-MAS) NMR spectrum showed about 50% of the bromo functional groups underwent the coupling reaction. Compared to the discrete, non-cross-linked cage compound 4, cage framework 14 exhibits more crystalline features according to the powder XRD analysis, and also shows greatly enhanced gas adsorption capacity, adsorbing 4-fold more CO₂ and 8 times more N₂. Relatively low ideal selectivity of 63/1 for adsorption of CO₂ over N₂ was observed with cage framework 14. In principle, by judiciously selecting a functionalized linker molecule that has stronger binding interactions with CO₂ than N₂, the gas adsorption selectivity of such framework structure can be further enhanced. To our knowledge, such cage-to-framework strategy has not yet been explored in the development of purely organic porous materials. Although a moderate degree of cross-linkage of cage molecules (4) was observed in our initial trial, we believe high conversion of functional groups in the discrete cage molecule can be achieved by varying the ratio of cage molecule to linker and reaction conditions (i.e., solvents, temperature etc.). A rich diversity of linker molecules and individual cage molecules with different properties can thus lead to the development of novel functional framework materials with distinct properties targeting specific applications, such as enhanced gas separation, heterogeneous catalysis, chemical sensing, and so forth.

Distortion of Molecular Cages. In our initial molecular design, we planned to control the cage pore size (distance between the top and bottom panels) by varying the length of three rigid lateral edges that connect the two trigonal panels through amine bonds. We expect to obtain molecular trigonal prisms with different heights (the distance between trigonal top and bottom panels). Compounds 5, 9, and 12 were designed as the lateral edges, with the distance of two aldehyde groups varying from 2.4, 5.0, to 11.9 Å respectively. However, it is interesting to note that computer modeling (Figure 4) as well as the solved crystal structure of cage 2 suggest that the two trigonal panels prefer to be twisted about 10–20°, and the rotation of one

trigonal panel with respect to the other leads to the reduction in the height of the prisms (Figure 5). Single crystals of cage 2 were obtained from a solution of 2 in 1:1:4 mixture of dichloromethane, ethyl acetate, and hexane. The single crystal X-ray analysis of 2 (Figure 4f) showed that the two trigonal panels twisted about 22°, and the distance between the top and the bottom panels is about 5.6 Å.³² Because of this type of distortion, cage 4 with the largest rigid lateral edges shows the smallest cavity size with the reduced prism height of 5.27 Å based on the energy-minimized molecular modeling study (Figure 4). Similar distortion of a trigonal prism toward a polyhedron with reduced height was also observed in a hexanuclear ruthenium coordination cage.⁴² The present trigonal prisms can adapt a distorted prismatic architecture due to the amine bond connection with rotational freedom. Such adaptability could lead to the development of responsive (breathable) cage-based organic porous materials.

Amino Group Density versus Pore Size. It is well accepted that adsorption of acidic CO₂ gas can be enhanced by introducing basic functionalities in the absorbent materials, and that the amino groups contribute significantly to the high capacity by showing favored interaction with CO₂.⁴³ Our gas adsorption studies showed that CO₂ uptake strongly depends on the amino group density in the cage molecule and is less sensitive to the cage pore size. Cage 2', which is constructed through imine bonds, shows comparable CO₂ adsorption capacity to the further reduced amine analogue 2. Density functional theory (DFT) calculations indicate that the adsorption energies for CO₂ on *N*-benzylaniline (C₆H₅CH₂NHC₆H₅) and *N*-benzyl-*N*-phenylimine (C₆H₅CH=NC₆H₅) are similar, −2.3 kcal/mol versus −2.2 kcal/mol. Cages (1–4, and 2') containing 6 nitrogen atoms in either amine or imine groups showed similar CO₂ uptake (~0.3 mol/mol) and the noncage analogue 13 which has only three amine groups adsorbs almost half as much CO₂ (0.18 mol/mol), compared to the corresponding cage analogue 2. Much higher CO₂ loading capacity (1.22 mol/mol) was observed in cage framework 14 than that in the other discrete cage molecules, which is presumably due to the facilitated transport of CO₂ to amine functional groups in the ordered framework structure 14. In terms of cubic centimeters per gram (cc/g) for the CO₂ adsorption, cage 4 with the largest molecular weight exhibits the lowest uptake, since the number of amino groups per gram of the material is much smaller (0.9 μmol/g, “amino group density”) than other cages.

In contrast to the uptake of CO₂, the experimental results suggest that the adsorption of nitrogen highly depends on the cage dimensions. We observed an increase in N₂ uptake with the

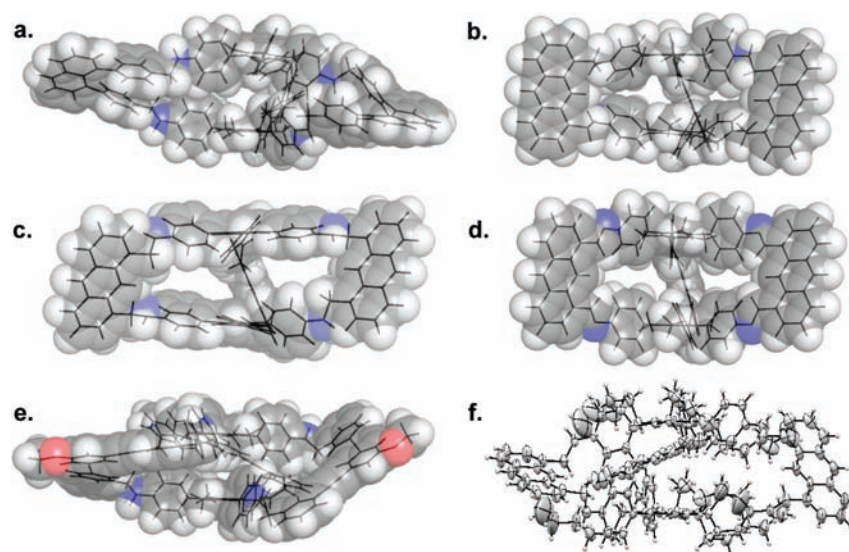


Figure 4. Energy-minimized molecular modeling and crystal structure: (a) cage 1; (b) cage 2; (c) cage 3; (d) cage 2'; (e) cage 4; (f) ORTEP drawing of cage 2 X-ray crystal structure. For cage 1, 2, 2', and 4, methyl group was used in calculation instead of hexyl for simplification. Panels a–e show the superimposition of space filling models with line models.

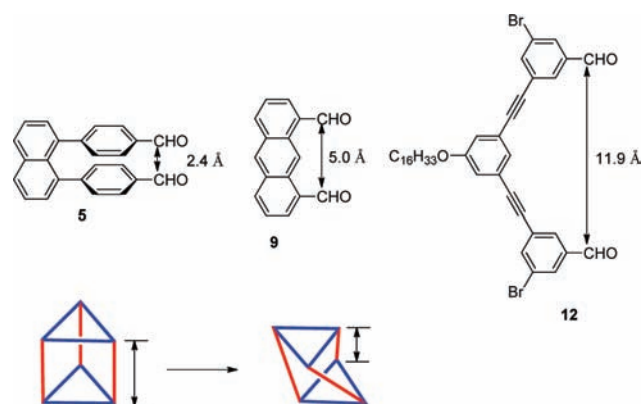


Figure 5. Rotation of the trigonal top panel along the threefold symmetry axis of the trigonal prism leads to the reduced prism height.

increase of cage pore size. For example, cage 4 with the smallest pore size of 5.27 Å (defined as the distance between the two trigonal panels) adsorbs the least amount of N₂, while the largest cage 2' (pore size 7.32 Å) adsorbs significantly larger amount of N₂. The unsubstituted cage 3 also showed an enhanced nitrogen adsorption capacity compared to its parent cage molecule 2, presumably due to the removal of six hexyl chains, which increased the effective gas binding surface area of the resulting porous materials. We also observed an almost 8-fold increase in the N₂ adsorption capacity of more ordered framework 14, compared to its parent cage 4, suggesting cross-linking of the discrete cage molecules can significantly enhance gas adsorption capacity.

The N₂ adsorption isotherms at 77 K showed these materials are nonporous to nitrogen gas with BET surface area less than 10 m²/g. Calculated pore size distribution for cage 3 showed that around one-third of the pores (by fraction of pore area) are 20 Å or larger, another third is between 20 and 16 Å, and the last third is 16 Å and smaller. Computational modeling study by inserting one nitrogen molecule into the molecular prisms was conducted

and the thermodynamic parameters were compared (Table S1). However, no clear correlation between the N₂–cage interaction energies and the pore size was observed. It should be noted that the accurate estimate of the adsorption energy was difficult due to the very low nitrogen adsorption energy (<1 kcal/mol), which may be close to the cage structure variation energy.

The gas adsorption selectivity could be attributed to both the amino group density of the cage molecule as well as the cage cavity size. The amino group density largely determines the CO₂ uptake, while N₂ adsorption capacity correlates to the dimensions of molecular prisms. Cage 4 exhibits the lowest nitrogen uptake, presumably due to its relatively smaller pore volume, while it shows comparable adsorption capacity for CO₂, thus, showing the highest CO₂/N₂ adsorption selectivity (138/1). Relatively low adsorption selectivity (63/1) of 14 for CO₂ over N₂ compared to that of the discrete cage 4 (138/1) is partially due to the introduction of phenyleneethynylene linker moieties that lack the favored binding interaction with CO₂. Further functionalization of the phenyleneethynylene linkers with multiple amino groups or other CO₂ binding sites is anticipated to further enhance the adsorption selectivity for CO₂ over N₂.

It remains unclear how gas molecules are adsorbed in these amorphous organic molecules. There exist both internal cavities (inside cages) as well as interstitial voids between independent cage molecules. It is likely that the gas molecules diffuse into both types of void spaces in the amorphous phase. The formation of the interstitial voids would be promoted by the prismatic shape of organic cage molecules, similar to the case of amorphous noria reported by Atwood et al.^{28c} The noncage analogue 13 has a very flexible molecular structure, which could alter the packing mode of the molecules dramatically. It is therefore not surprising that the noncage analogue 13 exhibits a different gas adsorption behavior, which does not follow the trend (selectivity, and capacity vs pore size) we observed for the other amorphous organic cages (1–4, and 2').

To achieve high CO₂/N₂ adsorption selectivity by using such organic-cage-based porous materials, an optimal balance of cage pore size and amino molar density is desired; larger pore volumes

would increase nitrogen adsorption and presumably increase adsorption rate, while higher amino group density would increase carbon dioxide adsorption capacity. Currently, systematically varying the molar density of the amino groups, exploring the adaptability of these cage compounds, and investigating the gas adsorption mechanism are being pursued in our lab. Further experimental and computational studies will deepen our understanding of the structure–property relationship between gas adsorption and cage composition.

CONCLUSIONS

A series of novel organic cage molecules were successfully synthesized in one pot from readily available starting materials and in high yield through imine condensation reaction. This study demonstrates the general applicability of such dynamic covalent chemical approach in constructing 3-D well-defined, structure-tunable molecular cages. A more ordered cage framework structure was obtained by covalent cross-linking of discrete cage building blocks. Remarkably, these 3-D cage compounds exhibit unprecedented high selectivity (up to 138/1) in adsorption of CO₂ over N₂, thus, showing great potential of these cage-based porous materials in gas separation and carbon capture applications. The cage molecules and the cage framework exhibited outstanding thermal stability with T_{dec} up to 710 K, thus, showing promise for gas separation applications at elevated temperatures. The structure–property relationship revealed a good correlation of CO₂ adsorption capacity to the amino group molar density of the cages, and the trend of higher N₂ adsorption capacity with increased cage pore size. Our study will shed light on some fundamental questions on the design principles of organic porous materials with high selectivity and capacity, and will also open many new possibilities for developing novel, application-specific, customizable cage-based porous materials.

EXPERIMENTAL SECTION

Synthesis. Representative preparative procedure and characterization data for cage **1** are given below. General experimental aspects, as well as procedures and characterization data for the other compounds, are available in Supporting Information.

Cage 1. To a solution of 1,3,5-trihexyl-2,4,6-tris(4-aminophenyl)benzene **11** (362 mg, 0.60 mmol) and 1,8-bis(4-formylphenyl)naphthalene (**5**) (304 mg, 0.90 mmol) in chloroform (200 mL) was added Sc(OTf)₃ (44 mg, 0.090 mmol) in CH₃CN (10 mL) dropwise. The yellow solution was stirred at room temperature for 24 h. NaBH(OAc)₃ (3.81 g, 18.0 mmol) was added, and the yellow suspension was stirred at room temperature for 5 h. The mixture was quenched by the addition of saturated NaHCO₃ (50 mL), and the organic layer was separated. The aqueous layer was extracted with CHCl₃ (3 × 50 mL). The combined organics were dried over Na₂SO₄ and concentrated to give the crude product. Purification by flash column chromatography (20% EtOAc in hexane as eluent) yielded the molecular cage **1** (570 mg, 90%) as a light yellow solid: ¹H NMR (500 MHz, CDCl₃) δ 7.97 (d, *J* = 8.2 Hz, 6H), 7.58 (t, *J* = 7.6 Hz, 6H), 7.44 (d, *J* = 7.0 Hz, 6H), 7.14 (d, *J* = 8.1 Hz, 6H), 7.10–7.00 (m, 24H), 6.82 (d, *J* = 8.2 Hz, 6H), 6.68 (dd, *J* = 8.1, 2.1 Hz, 6H), 6.52 (dd, *J* = 8.2, 2.1 Hz, 6H), 4.23 (s, 12H), 3.61 (s, 6H), 2.23–1.99 (m, 12H), 1.24–1.16 (m, 12H), 1.09–1.02 (m, 12H), 0.92–0.83 (m, 24H), 0.77 (t, *J* = 7.3 Hz, 18H); ¹³C NMR (101 MHz, CDCl₃) δ 146.70, 142.71, 140.34, 139.77, 139.23, 137.10, 135.67, 131.86, 131.60, 131.27, 130.71, 130.40, 129.63, 128.81, 126.69, 125.43, 112.74, 112.31, 49.25, 32.05, 31.24, 31.16, 29.81, 22.64, 14.48; MS (MALDI) calcd for C₁₅₆H₁₆₂N₆ ([M+]) 2120.29, found 2120.52.

Low-Pressure Gas Adsorption Measurements. Ideal gas adsorption measurements were performed using a custom-built stainless steel gas sorption apparatus specifically designed for small (100–200 mg) samples; containing a PX303-015ASV pressure transducer from Omega Engineering Corporation, a 47 mm membrane holder catalogue number XX4404700 from Millipore Corporation, and Swagelok tube fittings and valves. The data was acquired by a ADAC DaqBoard Pci5500MF from Abu Dhabi Airports Company and processed with Labview 7 Express from National Instruments. All samples were placed under vacuum between tests to remove all adsorbed gases, and kept at 20 °C for both adsorption testing and off-gassing phases. CO₂ and N₂ were used unaltered from Airgas, Inc. in single gas experiments for ideal gas adsorption; no mixed gas studies were performed.

Structure Modeling. Amber 10.0 program suite⁴⁴ was used to optimize cage molecular structures with semiempirical quantum mechanics method. For each cage, it was optimized in vacuum for 2500 steps using SCC-DFTB⁴⁵ and the conjugate gradient method. To obtain the N₂–cage interaction energy, for each cage, one N₂ molecule was put in the cage's pore and the overall structure was optimized using the same method. A dielectric constant of 1.0 was used during the minimization. We used Gaussian 09 program suite⁴⁶ to study the CO₂ adsorption on *N*-benzylaniline and *N*-benzyl-*N*-phenylimine. To calculate the CO₂ adsorption energy on *N*-benzylaniline, the structures of individual *N*-benzylaniline, individual CO₂, as well as the *N*-benzylaniline/CO₂ adsorption complex are optimized by B3LYP/6-31G* level of theory and their energies for the optimized structures, E_1 , E_2 , and E_3 , are obtained. Then, the adsorption energy $E_{ad} = E_3 - E_2 - E_1$. The CO₂ adsorption energy on *N*-benzyl-*N*-phenylimine can be calculated using a similar protocol.

ASSOCIATED CONTENT

Supporting Information. Experimental procedures, TGA, XRD, spectroscopic data, and theoretical calculations on gas adsorption energies. This material is available free of charge via the Internet at <http://pubs.acs.org>.

AUTHOR INFORMATION

Corresponding Author

Wei.Zhang@Colorado.edu

ACKNOWLEDGMENT

We thank Dr. Richard Shoemaker for solid state NMR assistance, University of Colorado innovative seed grant, and CRCW Junior Faculty Development award for funding support. This research used capabilities of the National Renewable Energy Laboratory Computational Sciences Center, which is supported by the Office of Energy Efficiency and Renewable Energy of the U.S. Department of Energy under Contract No. DE-AC36-08GO28308.

REFERENCES

- Yoshizawa, M.; Klosterman, J. K.; Fujita, M. *Angew. Chem., Int. Ed.* **2009**, *48*, 3418–3438.
- Leininger, S.; Olenyuk, B.; Stang, P. J. *Chem. Rev.* **2000**, *100*, 853–907.
- Mal, P.; Breiner, B.; Rissanen, K.; Nitschke, J. R. *Science* **2009**, *324*, 1697–1699.
- Iyer, K. S.; Norret, M.; Dalgarno, S. J.; Atwood, J. L.; Raston, C. L. *Angew. Chem., Int. Ed.* **2008**, *47*, 6362–6366.
- Hof, F.; Craig, S. L.; Nuckolls, C.; Rebek, J. *Angew. Chem., Int. Ed.* **2002**, *41*, 1488–1508.

- (6) Fujita, M.; Tominaga, M.; Hori, A.; Therrien, B. *Acc. Chem. Res.* **2005**, *38*, 369–378.
- (7) Thallapally, P. K.; McGrail, B. P.; Dalgarno, S. J.; Schaefer, H. T.; Tian, J.; Atwood, J. L. *Nat. Mater.* **2008**, *7*, 146–150.
- (8) Giles, M. D.; Liu, S. M.; Emanuel, R. L.; Gibb, B. C.; Grayson, S. M. *J. Am. Chem. Soc.* **2008**, *130*, 14430–14431.
- (9) Rowan, S. J.; Cantrill, S. J.; Cousins, G. R. L.; Sanders, J. K. M.; Stoddart, J. F. *Angew. Chem., Int. Ed.* **2002**, *41*, 898–952.
- (10) Lehn, J. M. *Chem.—Eur. J.* **1999**, *5*, 2455–2463.
- (11) (a) Zhang, W.; Moore, J. S. *Angew. Chem., Int. Ed.* **2006**, *45*, 4416–4439. (b) Zhang, W.; Moore, J. S. *J. Am. Chem. Soc.* **2004**, *126*, 12796–12796. (c) Ge, P.-H.; Fu, W.; Herrmann, W. A.; Herdtweck, E.; Campana, C.; Adams, R. D.; Bunz, U. H. F. *Angew. Chem., Int. Ed.* **2000**, *39*, 3607–3610. (d) Johnson, C. A., II; Lu, Y.; Haley, M. M. *Org. Lett.* **2007**, *9*, 3725–3728. (e) Jiang, J.; Tew, G. N. *Org. Lett.* **2008**, *10*, 4393–4396.
- (12) Jin, Y.; Zhang, A.; Huang, Y.; Zhang, W. *Chem. Commun.* **2010**, *46*, 8258–8260.
- (13) Icli, B.; Christinat, N.; Tonnemann, J.; Schuttler, C.; Scopelliti, R.; Severin, K. J. *J. Am. Chem. Soc.* **2009**, *131*, 3154–3155.
- (14) (a) Hartley, C. S.; Moore, J. S. *J. Am. Chem. Soc.* **2007**, *129*, 11682–11683. (b) Gallant, A. J.; MacLachlan, M. J. *Angew. Chem., Int. Ed.* **2003**, *42*, 5307–5310.
- (15) (a) Liu, X. J.; Warmuth, R. J. *J. Am. Chem. Soc.* **2006**, *128*, 14120–14127. (b) Liu, X.; Liu, Y.; Li, G.; Warmuth, R. *Angew. Chem., Int. Ed.* **2006**, *45*, 901–904. (c) Liu, X.; Warmuth, R. *Nat. Protocols* **2007**, *2*, 1288–1296.
- (16) (a) Tennyson, A. G.; Norris, B.; Bielawski, C. W. *Macromolecules* **2010**, *43*, 6923–6935. (b) Norris, B. C.; Sheppard, D. G.; Henkelman, G.; Bielawski, C. W. *J. Org. Chem.* **2011**, *76*, 301–304. (c) Norris, B. C.; Bielawski, C. W. *Macromolecules* **2010**, *43*, 3591–3593. (d) Hudnall, T. W.; Todd, W.; Bielawski, C. W. *J. Am. Chem. Soc.* **2009**, *131*, 16039–16041. (e) Williams, K. A.; Boydston, A. J.; Bielawski, C. W. *J. R. Soc. Interface* **2007**, *4*, 359–362. (f) Williams, K. A.; Bielawski, C. W. *Chem. Commun.* **2010**, *46*, 5166–5168.
- (17) D'aleandro, D. M.; Smit, B.; Long, J. R. *Angew. Chem., Int. Ed.* **2010**, *49*, 6058–6082.
- (18) Eddaoudi, M.; Moler, D. B.; Li, H. L.; Chen, B. L.; Reinecke, T. M.; O'Keeffe, M.; Yaghi, O. M. *Acc. Chem. Res.* **2001**, *34*, 319–330.
- (19) Murray, L. J.; Dinca, M.; Long, J. R. *Chem. Soc. Rev.* **2009**, *38*, 1294–1314.
- (20) Li, J. R.; Kuppler, R. J.; Zhou, H. C. *Chem. Soc. Rev.* **2009**, *38*, 1477–1504.
- (21) Wang, Z. Q.; Cohen, S. M. *Chem. Soc. Rev.* **2009**, *38*, 1315–1329.
- (22) Ma, L. Q.; Abney, C.; Lin, W. B. *Chem. Soc. Rev.* **2009**, *38*, 1248–1256.
- (23) Han, S. S.; Furukawa, H.; Yaghi, O. M.; Goddard, W. A. *J. Am. Chem. Soc.* **2008**, *130*, 11580–11581.
- (24) Schwab, M. G.; Fassbender, B.; Spiess, H. W.; Thomas, A.; Feng, X. L.; Mullen, K. J. *J. Am. Chem. Soc.* **2009**, *131*, 7216–7217.
- (25) Cooper, A. I. *Adv. Mater.* **2009**, *21*, 1291–1295.
- (26) McKeown, N. B.; Budd, P. M. *Chem. Soc. Rev.* **2006**, *35*, 675–683.
- (27) For reviews see: (a) McKeown, N. B. *J. Mater. Chem.* **2010**, *20*, 10588–10597. (b) Holst, J. R.; Trewin, A.; Cooper, A. I. *Nat. Chem.* **2010**, *2*, 915–920. (c) Cooper, A. I. *Angew. Chem., Int. Ed.* **2011**, *50*, 996–998.
- (28) (a) Atwood, J. L.; Barbour, L. J.; Jerga, A. *Science* **2002**, *296*, 2367–2369. (b) Thallapally, P. K.; Dalgarno, S. J.; Atwood, J. L. *J. Am. Chem. Soc.* **2006**, *128*, 15060–15061. (c) Tian, J.; Thallapally, P. K.; Dalgarno, S. J.; McGrail, P. B.; Atwood, J. L. *Angew. Chem., Int. Ed.* **2009**, *48*, 5492–5495.
- (29) Tozawa, T.; et al. *Nat. Mater.* **2009**, *8*, 973–978.
- (30) Sozzani, P.; Bracco, S.; Comotti, A.; Ferretti, L.; Simonutti, R. *Angew. Chem., Int. Ed.* **2005**, *44*, 1816–1820.
- (31) Lim, S.; Kim, H.; Selvapalam, N.; Kim, K. J.; Cho, S. J.; Seo, G.; Kim, K. *Angew. Chem., Int. Ed.* **2008**, *47*, 3352–3355.
- (32) Jin, Y. H.; Voss, B. A.; Noble, R. D.; Zhang, W. *Angew. Chem., Int. Ed.* **2010**, *49*, 6348–6351.
- (33) Mastalerz, M.; Schneider, M. W.; Opper, I. M.; Presly, O. *Angew. Chem., Int. Ed.* **2011**, *50*, 1046–1050.
- (34) (a) Ananchenko, G. S.; Udachin, K. A.; Dubes, A.; Ripmeester, J. A.; Perrier, T.; Coleman, A. W. *Angew. Chem., Int. Ed.* **2006**, *45*, 1585–1588. (b) Ananchenko, G. S.; Moudrakovski, I. L.; Coleman, A. W.; Ripmeester, J. A. *Angew. Chem., Int. Ed.* **2008**, *47*, 5616–5618.
- (35) de Lill, D. T.; Cahill, C. L. *Chem. Commun.* **2006**, 4946–4948.
- (36) The observed weight loss before the decomposition of framework **14** is presumably due to the remnant piperidine hydrobromide salt from the Sonogashira coupling reaction, and some grease involved from processing. The material was soaked in THF for 1 day and the NMR analysis of the solution phase showed the presence of piperidine hydrobromide and grease.
- (37) For recent studies on the CO₂/N₂ selectivities of some other porous materials, see: (a) Keskin, S.; Sholl, D. S. *Ind. Eng. Chem. Res.* **2009**, *48*, 914–922. (b) Bastin, L.; Barcia, P. S.; Hurtado, E. J.; Silva, J. A. C.; Rodrigues, A. E.; Chen, B. *J. Phys. Chem. C* **2008**, *112*, 1575–1581.
- (38) Thallapally, P. K.; McGrail, B. P.; Atwood, J. L.; Gaeta, C.; Tedesco, C.; Neri, P. *Chem. Mater.* **2007**, *19*, 3355–3357.
- (39) Park, H. J.; Suh, M. P. *Chem.—Eur. J.* **2008**, *14*, 8812–8821.
- (40) Jiang, J. X.; Su, F.; Trewin, A.; Wood, C. D.; Campbell, N. L.; Niu, H.; Dickinson, C.; Ganin, A. Y.; Rosseinsky, M. J.; Khimyak, Y. Z.; Cooper, A. I. *Angew. Chem., Int. Ed.* **2007**, *46*, 8574–8578.
- (41) Swamy, S. I.; et al. *J. Am. Chem. Soc.* **2010**, *132*, 12773–12775.
- (42) Mirtschin, S.; Slabon-Turski, A.; Scopelliti, R.; Velders, A. H.; Severin, K. J. *J. Am. Chem. Soc.* **2010**, *132*, 14004–14005.
- (43) Arnone, A. *Nature* **1974**, *247*, 143–145.
- (44) Case, D. A. D. et al. *AMBER 10*; University of California: San Francisco, CA, 2008.
- (45) Elstner, M.; Porezag, D.; Jungnickel, G.; Elsner, J.; Haugk, M.; Frauenheim, T.; Suhai, S.; Seifert, G. *Phys. Rev. B* **1998**, *58*, 7260–7268.
- (46) Frisch, M. J.; et al. *Gaussian 09*, Revision A.2; Gaussian, Inc.: Wallingford, CT, 2009.